Erratum

Pulsed jet dynamics of squid hatchlings at intermediate Reynolds numbers

Ian K. Bartol, Paul S. Krueger, William J. Stewart and Joseph T. Thompson

There were several errors published in *J. Exp. Biol.* **212**, 1506-1518.

On p. 1507, in paragraph 4 of the Introduction, the fourth and fifth sentences read:

Moreover, for a fixed $\hat{U}$, $Re \propto L_b$. Thus, weight-specific drag is proportional to $Re^{-1/2}$ at high Re and $1/Re^{-1/2}$ at low Re for swimming at a fixed speed in body lengths s^{-1}.

The text should have read:

Moreover, for a fixed $\hat{U}$, $Re \propto L_b^2$. Thus, weight-specific drag is proportional to $Re^{1/2}$ at high Re and $Re^{-1/2}$ at low Re for swimming at a fixed speed in body lengths s^{-1}.

We apologise to authors and readers for this error.

Pulsed jet dynamics of squid hatchlings at intermediate Reynolds numbers

Ian K. Bartol[1,*], Paul S. Krueger[2], William J. Stewart[1] and Joseph T. Thompson[3]

[1]Department of Biological Sciences, Old Dominion University, Norfolk, VA 23529, USA, [2]Department of Mechanical Engineering, Southern Methodist University, Dallas, TX 75275, USA and [3]Department of Biology, Franklin and Marshall College, Lancaster, PA 17604, USA

*Author for correspondence (e-mail: ibartol@odu.edu)

SUMMARY

Squid paralarvae (hatchlings) rely predominantly on a pulsed jet for locomotion, distinguishing them from the majority of aquatic locomotors at low/intermediate Reynolds numbers (Re), which employ oscillatory/undulatory modes of propulsion. Although squid paralarvae may delineate the lower size limit of biological jet propulsion, surprisingly little is known about the hydrodynamics and propulsive efficiency of paralarval jetting within the intermediate Re realm. To better understand paralarval jet dynamics, we used digital particle image velocimetry (DPIV) and high-speed video to measure bulk vortex properties (e.g. circulation, impulse, kinetic energy) and other jet features [e.g. average and peak jet velocity along the jet centerline (U_j and U_{jmax}, respectively), jet angle, jet length based on the vorticity and velocity extents (L_ω and L_V, respectively), jet diameter based on the distance between vorticity peaks (D_ω), maximum funnel diameter (D_F), average and maximum swimming speed (U and U_{max}, respectively)] in free-swimming _Doryteuthis pealeii_ paralarvae (1.8 mm dorsal mantle length) (Re_{squid}=25–90). Squid paralarvae spent the majority of their time station holding in the water column, relying predominantly on a frequent, high-volume, vertically directed jet. During station holding, paralarvae produced a range of jet structures from spherical vortex rings (L_ω/D_ω=2.1, L_V/D_F=13.6) to more elongated vortex ring structures with no distinguishable pinch-off (L_ω/D_ω=4.6, L_V/D_F=36.0). To swim faster, paralarvae increased pulse duration and L_ω/D_ω, leading to higher impulse but kept jet velocity relatively constant. Paralarvae produced jets with low slip, i.e. ratio of jet velocity to swimming velocity (U_j/U or U_{jmax}/U_{max}), and exhibited propulsive efficiency [η_{pd}=74.9±8.83% (±s.d.) for deconvolved data] comparable with oscillatory/undulatory swimmers. As slip decreased with speed, propulsive efficiency increased. The detection of high propulsive efficiency in paralarvae is significant because it contradicts many studies that predict low propulsive efficiency at intermediate Re for inertial forms of locomotion.

Key words: squid, hydrodynamics, locomotion, low Reynolds number, propulsive efficiency, vortex rings.

INTRODUCTION

Studies of aquatic biological locomotion at low and intermediate Reynolds numbers (Re=10^0–10^3) have been performed on a variety of taxa, such as fish larvae (Fuiman and Batty, 1997; Müller and Videler, 1996; Vlyman, 1974; Weihs, 1980), ascidian larvae (McHenry et al., 2003), copepods (Catton et al., 2007; Malkiel et al., 2003; van Duren and Videler, 2003; Yen and Fields, 1992), pteropods (Borell et al., 2005), brine shrimp (Williams, 1994) and damsel-fly larvae (Brackenbury, 2002). Whereas the organisms above propel themselves using oscillatory/undulatory motions of various appendages, squid paralarvae (hatchlings) employ a pulsed jet for locomotion at intermediate Re. [The term paralarvae is used because squid hatchlings exhibit behavioral and ecological characteristics that distinguish them from adults but unlike the larvae of many other invertebrates, they do not undergo radical metamorphosis during post-hatching development (Boletzky, 1974; Young and Harman, 1988)]. This fundamentally different propulsive mechanism, i.e. jetting, involves (1) radial expansion of the mantle, resulting in the inflow of water into the mantle cavity through anterior intakes, followed by (2) the contraction of circular muscles in the mantle, which increases the pressure in the mantle cavity, closes valves on the intake slots and drives water out of the mantle cavity _via_ the funnel (Fig. 1). This pattern is repeated to produce a pulsed jet. Although paralarvae have fins, which are an important secondary propulsive mechanism in juvenile and adult squid (Hoar et al., 1994; Bartol et al., 2001a; Bartol et al., 2001b; Anderson and

DeMont, 2005; W.J.S., I.K.B. and P.S.K., in preparation), they are rudimentary and appear to play little role in propulsion during early life-history stages (Boletzky, 1987; Hoar et al., 1994).

Pulsed jetting has two important components that play integral roles in thrust production. The first component is the impulse per pulse supplied by the jet momentum flux (I_U) and the second component is the impulse per pulse supplied by the nozzle exit over-pressure (I_P), i.e. fluid pressure above the local ambient pressure during jet ejection. These components relate to time-averaged thrust ($\bar{F}_T$) as follows (Krueger and Gharib, 2003):

$$\bar{F}_T = \frac{1}{T}\left(I_U + I_P\right),\qquad(1)$$

where T is the period between successive jets. For steady sub-sonic jets, I_P=0 but for unsteady jets, such as those found in squid paralarvae, I_P can be substantial, contributing as much as 42% to the total impulse of the jet (Krueger, 2001; Krueger and Gharib, 2003).

Toroidal fluid masses, known as vortex rings, are the critical coherent structures for the production of I_P and thus directly relate to propulsive performance. During vortex ring formation, ambient fluid is accelerated by entrainment and added mass effects, resulting in increased nozzle exit over-pressure (Krueger and Gharib, 2003). This important observation was made using a mechanical piston-cylinder apparatus that produced jet pulses in stationary water (Re~10^4). In a related study, Gharib et al. determined that there was
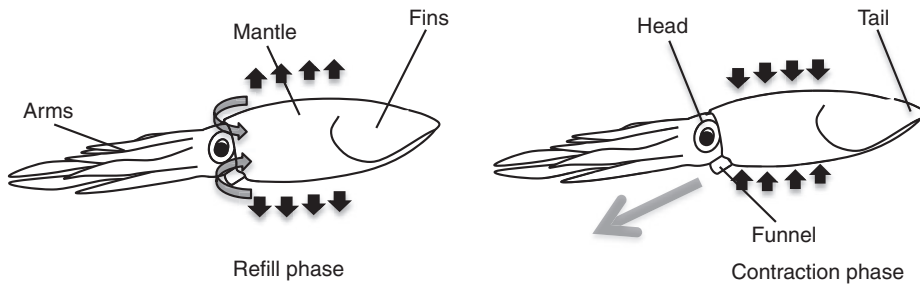
Fig. 1. Illustration of squid and relevant structures during mantle cavity refilling (left) and mantle contraction (right). The black arrows indicate movement of the mantle.

a specific stroke ratio [stroke ratio is defined as the length of the ejected plug of fluid (L) to the diameter of the jet aperture (D)] where vortex rings stop forming midway through the pulse and pinch-off from the trailing jet in terms of entrainment of circulation (Gharib et al., 1998). After the ring pinches off, the remainder of the jet contributes little to I_P and behaves essentially like a steady jet. The specific stroke ratio where pinch-off occurs is called the formation number (F).

The concepts of vortex ring formation, impulse and stroke ratio have high relevance for unsteady jetting in squids at intermediate Re where the dependence of drag on Re changes significantly. The weight-specific drag is proportional to $C_D L_b \hat{U}^2$ where C_D is the drag coefficient, $\hat{U}$ is the swimming speed normalized in body lengths s^{-1} and L_b is the body length. At high Re, C_D is approximately constant but $C_D \propto 1/Re$ as Re drops below one and the role of viscosity becomes dominant. Moreover, for a fixed $\hat{U}$, $Re \propto L_b$. Thus, weight-specific drag is proportional to $Re^{-1/2}$ at high Re and $1/Re^{-1/2}$ at low Re for swimming at a fixed speed in body lengths s^{-1}. Using the known drag coefficient of a sphere (White, 2006) as representative of the expected trend in C_D with Re, the transition from decreasing to increasing weight-specific drag as Re decreases occurs in the intermediate Re range (10–100). To combat the trend toward a relative increase in drag as Re decreases into the intermediate range, a relative increase in thrust would be beneficial. This could be achieved by using short pulses with stroke ratios less than or approximately equal to F, where high Re jets in quiescent fluid have shown maximum impulse per pulse (Krueger and Gharib, 2003).

Augmenting thrust, however, tends to be problematic in that additional kinetic energy is injected into the wake as thrust is increased (for a fixed jet diameter), leading to potentially lower propulsive efficiency. Nevertheless, recent results from adult squid (Bartol et al., 2009) have shown that conditions for improved thrust per pulse (i.e. jet pulses with stroke ratios close to or smaller than F) also lead to improved propulsive efficiency. Therefore, the benefit of thrust augmentation from vortex ring formation seemingly outweighs the kinetic energy penalty under these conditions. Clearly similar results may benefit paralarval propulsion, especially as their smaller size implies limited energy reserves, but it is not known if these observations continue to hold at intermediate Re because vortex ring formation may be altered by the increased role of viscosity. In addition to the (potential) benefits of vortex ring formation, a larger funnel diameter can improve propulsive efficiency at intermediate Re by providing the same thrust with a lower jet velocity.

Known characteristics of paralarval squid support the expectations that short jet pulses and large funnel diameters are beneficial for locomotion at intermediate Re. Paralarval squid do indeed have relatively large funnel complexes compared with larger juveniles and adults (Packard 1969; Boletzky, 1974; Thompson and Kier, 2002), which may be beneficial for propulsive efficiency as described above. Moreover, there is evidence that *Sepioteuthis lessoniana* hatchlings have higher mantle contraction rates than

juveniles or adults during escape jetting (Thompson and Kier, 2001; Thompson and Kier, 2006), potentially leading to short stroke ratios less than or equal to F that can improve both thrust and propulsive efficiency. Interestingly, Thompson and Kier found that weight-specific peak thrust and impulse of the escape jet are significantly lower for smaller hatchlings than juveniles or sub-adults (Thompson and Kier, 2002). This apparent deviation from the predictions above may be a product of escape jetting occurring near the high end of the intermediate Re number range, where the weight-specific drag transition has not been fully realized.

Despite the potential relationships among vortex ring formation, impulse and stroke ratio during pulsed jetting at intermediate Re, little is known about jet flows produced by squid hatchlings. Specifically, do paralarvae produce vortex rings at these scales? How fast is water expelled relative to swimming velocities and what stroke ratios are observed? How efficient is the jet in these small worlds? In the present study we seek to answer these questions by using digital particle image velocimetry (DPIV) to directly measure bulk ring properties (e.g. circulation, impulse, kinetic energy) and other jet features (e.g. L/D, jet velocity, vorticity structure) in free-swimming paralarval *Doryteuthis pealeii* [formerly *Loligo pealeii* (see Vecchione et al., 2005)]. Although some of the questions above were addressed briefly in a previously published overview paper on squid jetting throughout ontogeny (see Bartol et al., 2008), we present a more detailed and expansive data set in this paper.

MATERIALS AND METHODS
Animals and maintenance
Doryteuthis pealeii Lesueur eggs were purchased from the Marine Biological Laboratory, Woods Hole, MA, USA. The eggs were maintained in a re-circulating seawater holding system (610l) at a salinity of 30–32psu using synthetic sea salts (Instant Ocean®, Spectrum Brands, Atlanta, GA, USA) and a water temperature of 16–19°C. Within the holding system, the eggs were kept in 18.9l buckets positioned on the tank bottom with the bucket rims projecting above the water line. To permit circulation of flow through the buckets, a series of 5cm diameter holes were drilled along the bucket sides and covered with 0.5mm mesh. Upon hatching, which generally occurred overnight, the paralarvae were transferred using a modified pipette to smaller (0.25l) plastic containers that also allowed water exchange *via* a meshed hole arrangement. These containers, which floated at the water surface *via* aquarium tubing wrapped around their edges, were used to separate paralarvae according to hatching time. Only those paralarval *D. pealeii* [1.8mm dorsal mantle length (*DML*)] <12h old (post-hatching) were used in experiments.

DPIV experiments
A total of 36 trials were performed; each experimental trial consisted of 4–28 recording periods, within which 2–11 jet sequences were recorded. For each experimental trial, 1–6 paralarvae were added to a Plexiglas holding chamber (4.0×6.0×2.5cm) (125 animals were

considered in total) and were allowed to acclimate for 5 min prior to experimentation. Multiple squid were added to the chamber to increase the probability of imaging a free-swimming paralarvae within a limited field of view. The chamber was filled with seawater (30–32 psu, 16–19°C) seeded with neutrally buoyant, silver-coated, hollow glass spheres (mean diameter=14 μm, Potters Industries, Valley Forge, PA, USA). The spheres were illuminated with a 0.5–2.0 mm thick (with aperture and without aperture, respectively) parasagittal plane using two (A and B) pulsed ND:YAG lasers and a laser optical arm (wavelength=532 nm, power rating= 350 mJ pulse^{-1}; LaBest Optronics, Beijing, China). Each laser was operated at 15 Hz (7 ns pulse duration) with a 1–4 ms separation between laser A and B pulses.

A UP-1830CL, 8-bit, 'double-shot' video camera (1024×1024 pixel resolution, paired images collected at 15 Hz; UNIQ Vision, Santa Clara, CA, USA) outfitted with a VZM 450i zoom lens (Edmund Optics, Barrington, NJ, USA) was used for DPIV data capture. The camera was positioned orthogonally to the laser plane to record movements of particles around paralarval squid (1.8×1.8 cm field of view). Fine scale focusing and movement of the camera were achieved using a series of optical stages (Optosigma, Santa Ana, CA, USA). A high-speed 1M150 video camera (1024×1024 pixel resolution, frame rate set at 100 Hz; DALSA, Waterloo, ON, Canada) outfitted with a Fujinon CF25HA-1 25 mm lens (Fujinon, Inc., Wayne, NJ, USA) and positioned laterally to the holding chamber was used to record swimming motions of the paralarvae. Transfer of video frames from the UNIQ and DALSA cameras to hard disk was accomplished using two CL-160 capture cards and VideoSavant 4.0 software (IO Industries, London, ON, Canada).

Separate lighting and spectral filters were used with each camera. A series of four 40 W lights outfitted with a color gel #27 filter (transmits wavelengths >600 nm) provided illumination for the high-speed DALSA camera whereas the laser light (532 nm) provided the illumination for the DPIV UNIQ camera. A Kodak Wratten 32 magenta filter (blocks wavelengths 520–600 nm) was mounted to the DALSA camera lens to prevent overexposure of laser light, and an IR filter and a Kodak Wratten 58 green filter (transmits wavelengths of 410–600 nm) were mounted to the UNIQ UP-1830CL camera lens to prevent overexposure from the 40 W halogen lights.

The lasers and DPIV camera were triggered and synchronized using a timing program developed by Dr Morteza Gharib's Lab (California Institute of Technology, Pasadena, CA, USA), a PCI-6602 counter/timing card (National Instruments, Austin, TX, USA) and a BNC-565 pulse generator (Berkeley Nucleonics, San Rafael, CA, USA). A 4003A signal generator (B&K Precision, Yorba Linda, CA, USA) was used to trigger the DALSA camera at 100 Hz. Although the DPIV and high-speed cameras collected data at different frame rates, recording time durations were kept constant using the VideoSavant acquisition software.

For analysis of the DPIV data, each image was subdivided into a matrix of 32^2 pixel interrogation windows. Using a 16 pixel offset (50% overlap), cross-correlation was used to determine the particle displacements within interrogation windows on the paired images using *PixelFlow*^{TM} software (FG Group LLC, San Marino, CA, USA) (Willert and Gharib, 1991). Outliers, defined as particle shifts that were 3 pixels greater than their neighbors, were removed and the data were subsequently smoothed to remove high-frequency fluctuations. Window shifting was performed followed by a second iteration of outlier removal and smoothing (Westerweel et al., 1997). Using *PixelFlow*^{TM} software, velocity vector and vorticity contour fields were determined. Circulation was calculated by integrating vorticity within the lowest iso-vorticity contour level consistent with the quality of the data, which generally occurred around 10% of peak vorticity.

Velocity vector fields, vorticity contour fields and circulation were calculated for all experimental trials and these data were used to select 33 representative jet sequences for further kinematic and propulsive efficiency analyses, which are described below. For all 33 jet sequences, paralarvae were at least 1 cm (~5 *DML*) from the holding chamber walls and water surface.

Kinematic measurements

Detailed frame-by-frame position tracking of hatchlings in the high-speed footage of the 33 swimming sequences was performed using the National Institute of Health's public domain program ImageJ (http//rsb.info.nih.gov/ij/) and Matlab code written by T. Hedrick (University of North Carolina, Chapel Hill, NC, USA, available at http://www.unc.edu/~thedrick/software1.html). The positional information was used to measure displacement during the contraction and refilling phases of the jet cycle and to compute average and peak swimming speeds for representative DPIV sequences. Mantle contraction periods, refill periods, maximum funnel diameter (D_F) and fin beats were also determined from the high-speed footage.

Jet properties

The DPIV method provides full-field velocity measurements in a planar cross-section of the 3-dimensional (3-D) flow. Because axisymmetry of the jet flow was assumed for simplicity, it was not necessary to resolve the full 3-D flow field data for our calculations of jet properties, which were performed using a suite of analysis tools developed in Matlab (The Mathworks, Inc., Natick, MA, USA), including graphical user interface features to allow for user control over the data processing procedure.

For analysis of jet flows, the region of the flow containing the jet was identified based on the vorticity field and the following operations were performed for each frame in the selected jet sequence: (1) The location of the jet centerline and the components of the unit vectors in the longitudinal $\hat{\mathbf{n}}_z$ and radial $\hat{\mathbf{n}}_r$ directions relative to the jet centerline (see Fig. 2) were computed using one of two user-selected methods. (i) For method 1, the jet centerline was centered on the centroid of the jet region over which the jet velocity magnitude was above a specified threshold (generally ~20% of peak jet velocity). The orientation (slope) of the jet centerline was determined from the weighted average of the jet velocity vector orientation in the same region used to identify the jet centroid. This method worked well for longer jets. (ii) For method 2, the jet centerline was centered between the locations of the positive and negative peak vorticity and was oriented perpendicular to the line connecting the vorticity peaks. The locations of the vorticity peaks were determined from the centroids of vorticity with magnitude greater than a specified threshold (generally ~20% of peak jet vorticity). This method worked well for shorter jets. Unit vectors were then computed from the known centerline orientation. (2) Using the angled centerline as the r=0 axis, the magnitude of the jet impulse (I) and the excess kinetic energy of the jet (E) were computed from:

$$I / \rho = \pi \int_{\text{jet}} \omega_\theta r^2 dr\, dz \;, \qquad (2)$$

$$E / \rho = \pi \int_{\text{jet}} \omega_\theta \psi\, dr\, dz \;, \qquad (3)$$

where ω_θ is the azimuthal component of vorticity, r is the radial coordinate, z is the longitudinal coordinate along the jet axis, ψ is

Fig. 2. Convolved (A,C) and deconvolved (B,D) velocity and vorticity fields for a paralarval *Doryteuthis pealeii* swimming at 1.3 cm s^{-1} (7.0 *DML* s^{-1}). η_p is the propulsive efficiency, r is the radial coordinate relative to the jet centerline, z is the longitudinal coordinate along the jet axis, $\hat{n}_r$ is the unit vector in the radial direction relative to the jet centerline, $\hat{n}_z$ is the unit vector in the longitudinal direction relative to the jet centerline and *DML* is the dorsal mantle length.

the Stokes stream function, and ρ is the fluid density. The area integrals were computed using a 2-D version of the trapezoidal rule. The effects of the velocity field around the vortex (not induced by the vortex itself) were considered to have negligible influence on impulse calculations because all vortices considered in our analysis were spaced more than three ring diameters away from other vortices or boundaries. Although multiple squid were occasionally observed in the field of view, only sequences involving a single hatchling were considered in these analyses. (3) The components of the impulse vector in the vertical and horizontal directions were computed based on the direction of $\hat{n}_z$ relative to the horizontal. (4) The length of the jet was computed based on the extent over which the centerline velocity magnitude was above a specified threshold (L_V) and the extent over which the jet vorticity field was above a specified magnitude (L_ω). (5) The mean (U_j) and peak (U_{jmax}) jet velocity along the jet centerline were computed. (6) The jet diameter was determined based on the distance between vorticity peaks perpendicular to the jet centerline (D_ω).

After computation of the jet parameters listed above, I, D_ω, L_V and L_ω were overlaid on a vorticity plot for each frame in the jet sequence, allowing the user to visually check the data and allow for correction of input parameters as necessary. Mean values for D_ω, L_V and L_ω were computed for the jet sequence and these mean values are presented in the remainder of the paper.

Using the direction of squid motion during mantle contraction, which was measured using the high-speed kinematic data, and the jet angle to the horizontal determined from $\hat{n}_z$, the component of the impulse aligned with the direction of displacement was computed.

Propulsive efficiency

Because paralarvae are strongly negatively buoyant, tending to sink rapidly during refilling, and work done by the propulsive system – not work done by gravity – is of interest, the effect of gravity on the net motion was factored out by considering only the motion during jet ejection. Consequently, propulsive efficiency (η_p) was computed for only the exhalant phase of the jet cycle using the equation:

$$\eta_p = \frac{\tilde{F}_T x}{\tilde{F}_T x + E} , \qquad (4)$$

where $\tilde{F}_T$ is the jet thrust time-averaged over the mantle contraction and x is displacement during mantle contraction. $\tilde{F}_T$ was determined by dividing the impulse component in the direction of displacement by the mantle-contraction period. The impulse was the mean of impulse measurements over several frames after jet termination; the excess kinetic energy was the peak excess kinetic measurement after jet termination within the sequence of frames.

Correction for laser sheet thickness

For the present study, the thickness of the laser sheet (t) and the funnel diameter were comparable due to limitations in the laser optics used for the formation of the laser sheet. Because the velocity field measurements were depth averaged over t (0.5–2.0 mm), measured jet velocities and peak vorticities were below actual values.

Mathematically, the depth averaging effect may be expressed as a convolution operation, namely:

$$\langle f \rangle = \int_{0}^{\infty} k(r) f(z,r) \, dr , \qquad (5)$$
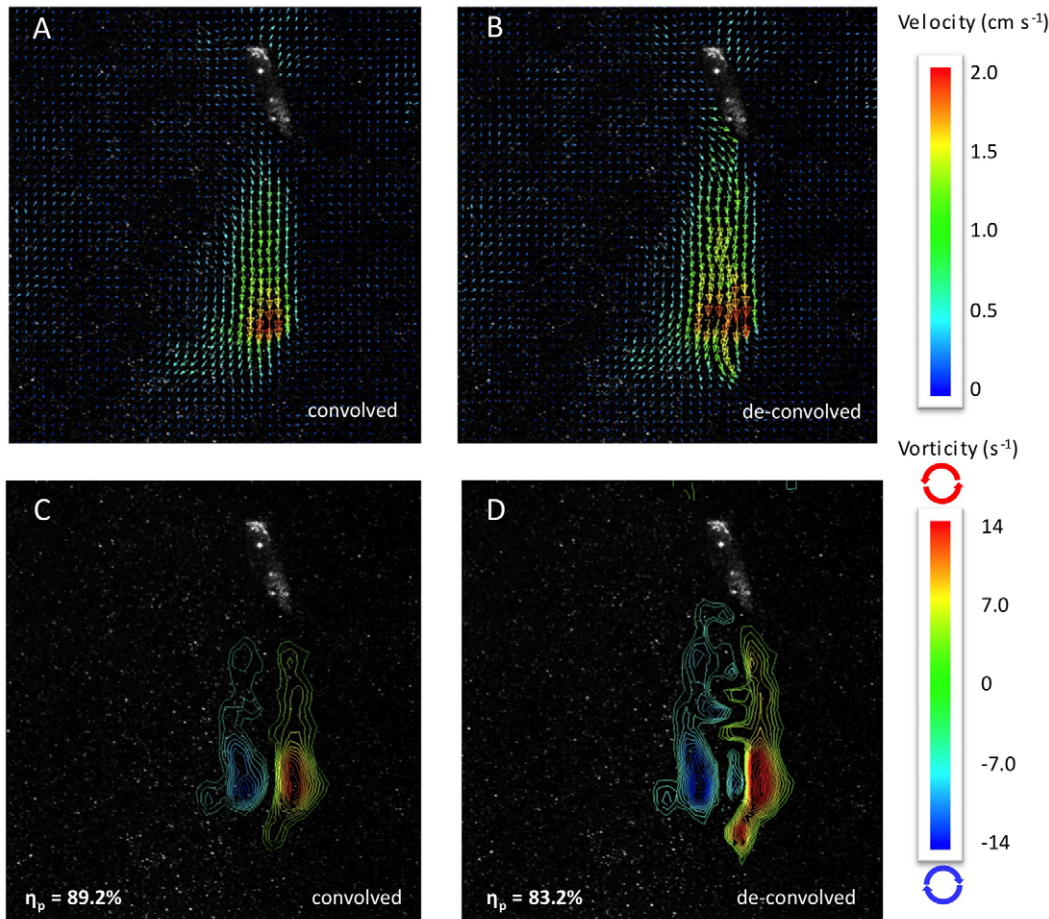
Fig. 3. Convolved (A,C) and deconvolved (B,D) velocity and vorticity fields for a paralarval *Doryteuthis pealeii* swimming at 1.8 cm s^{-1} (10.0 *DML* s^{-1}). η$_p$ is the propulsive efficiency and *DML* is the dorsal mantle length.

where *f* is the actual data field being averaged (convolved) and *k* is the convolution kernel. The DPIV imaging processing provides equal treatment of particles within the laser sheet, regardless of the beam profile. Therefore, for the axial velocity, which is measured directly, we set $f=u_z$ and $k=1$ within the laser sheet and $k=0$ elsewhere, giving:

$$\langle u_z \rangle(z,r) = \int_r^{r+t/2} u_z(z,r')\,dr' ,\qquad(6)$$

where $\langle u_z \rangle$ is the convolved (i.e. measured) axial velocity and u_z is the actual axial velocity of the jet. For the radial velocity, u_r, only the vertical component is measured with DPIV, so we set $k=\cos[\theta_r(\tau)]$ within the laser sheet and $k=0$ elsewhere. Here, $\theta_r(\tau)$ is the angle between the 3-D radial direction relative to the jet axis and the vertical plane of the center of the laser sheet at location τ within the laser sheet. Using this convolution kernel, the convolution operation for the radial velocity becomes:

$$\langle u_r \rangle(z,r) = \int_r^{r+t/2} \cos[\theta_r(r')]\,u_r(z,r')\,dr' .\qquad(7)$$

The convolution of the velocity data over *t* is expected to lower the computed impulse and kinetic energy values. To remove this effect, the data were deconvolved using an iterative algorithm that reproduced the actual velocity components u_z and u_r to within a specified tolerance (usually set to 1% of the peak jet velocity). The algorithm was exact to within the specified tolerance under the

assumption of axisymmetry of the underlying velocity fields u_z and u_r. Deconvolution of all the paralarval velocity fields were used to obtain more accurate values of *I*, *E*, U_j and U_{jmax}.

RESULTS
Swimming behaviors

All of the data reported in the present study are for tail-first swimming, the preferred mode of locomotion in paralarval *D. pealeii,* and all means are reported as means ±1 s.d. The paralarvae spent much of their time 'station holding' or 'vertically bobbing' in the water column, especially near the water surface. However, only those sequences where paralarvae swam >1 cm away from the water surface and holding chamber walls were considered in the present analysis because surface station holding often involved breaching and rapid decelerations, behaviors that complicate propulsive efficiency calculations. During water column station holding, paralarvae ascended during mantle contraction and descended during mantle refilling, with the duration of the refill period largely determining net vertical displacement in the water column. The mean contraction period was 0.092±0.016 s, comprising on average only 23.34±7.67% of the total jet period. The mean total jet period (contraction and refilling) was 0.41±0.08 s.

The mean peak swimming speed was 2.68±0.85 cm s^{-1} (14.74±4.56 *DML* s^{-1}) during mantle contraction with a range of 1.46–4.84 cm s^{-1} (4.98–26.87 *DML* s^{-1}), and the mean average swimming speed during contraction was 1.56±0.56 cm s^{-1} (8.70±3.12 *DML* s^{-1}) with a range of 0.66–3.05 cm s^{-1} (3.67–16.94 *DML* s^{-1}). The mean jet (funnel) angle (relative to

horizontal) was 84.25±5.79 deg. with a range of 67.1–90.0 deg. The vertically directed jet can be seen in the velocity plots of Figs 2 and 3.

During the majority of the swimming sequences, one fin downstroke coincided with each mantle contraction, with the fins moving upward during the refilling phase. Based on the high-speed footage, it was not clear whether these fin motions were passive or active. However, DPIV data reveal negligible impulse production from these motions, although greater spatial resolution is probably necessary to fully resolve the fin flows. Moreover, previous observations indicate that paralarvae sink rapidly during the refilling phase even when the fins are in motion (Bartol et al., 2008). Therefore, irrespective of whether these motions are passive or active, fin force production is probably very low relative to the jet.

Adjustment for laser thickness

As indicated in the Materials and methods, an algorithm was developed to deconvolve the velocity and vorticity fields to correct for depth-averaging of the data by t. L_V, L_ω and D_ω were similar for both convolved and deconvolved calculations (within ~6–8% of one another). However, because the Matlab routines did slightly better at matching convolved parameters with the vorticity field (based on visual comparisons of the computed values with the vorticity fields for each case), convolved values for L_V, L_ω and D_ω were considered more reliable and are presented in subsequent sections. By contrast, I, E, U_j and U_{jmax} were significantly different in convolved and deconvolved calculations and thus deconvolved values for I, E, U_j and U_{jmax} are presented for the remainder of the paper unless stated otherwise. Convolved and deconvolved data are illustrated in Figs 2 and 3. Although the velocity and vorticity fields do increase in magnitude during the deconvolution process as expected, the general shape of the velocity and vorticity fields are similar. The deconvolved velocity and vorticity fields show some irregularity near the centerline, which is a result of the deconvolution process amplifying non-axisymmetric features near the centerline (the centerline being most heavily affected by the deconvolution). These irregular features have minimal effect when calculating I, E, U_j and U_{jmax} because I and E are weighted toward data off of the centerline (see Eqns 2 and 3, noting that $\psi \rightarrow 0$ as $r \rightarrow 0$) and they are averaged out in the computation of U_j and U_{jmax}. For clarity, we present both the convolved and deconvolved vorticity plots in Fig. 4 so that any irregularity in the deconvolved data does not detract from the general vorticity patterns.

DPIV and jet properties

Over the Re range considered in this study [Reynolds number of jet (Re_{jet})=5–25, Reynolds number of squid (Re_{squid})=25–90], a continuum of jet structures was observed. The jet structures ranged from spherical vortex rings (L_ω/D_ω=2.1, L_V/D_F=13.6) to more elongated vortex ring structures with tails (L_ω/D_ω=4.6, L_V/D_F=36.0)
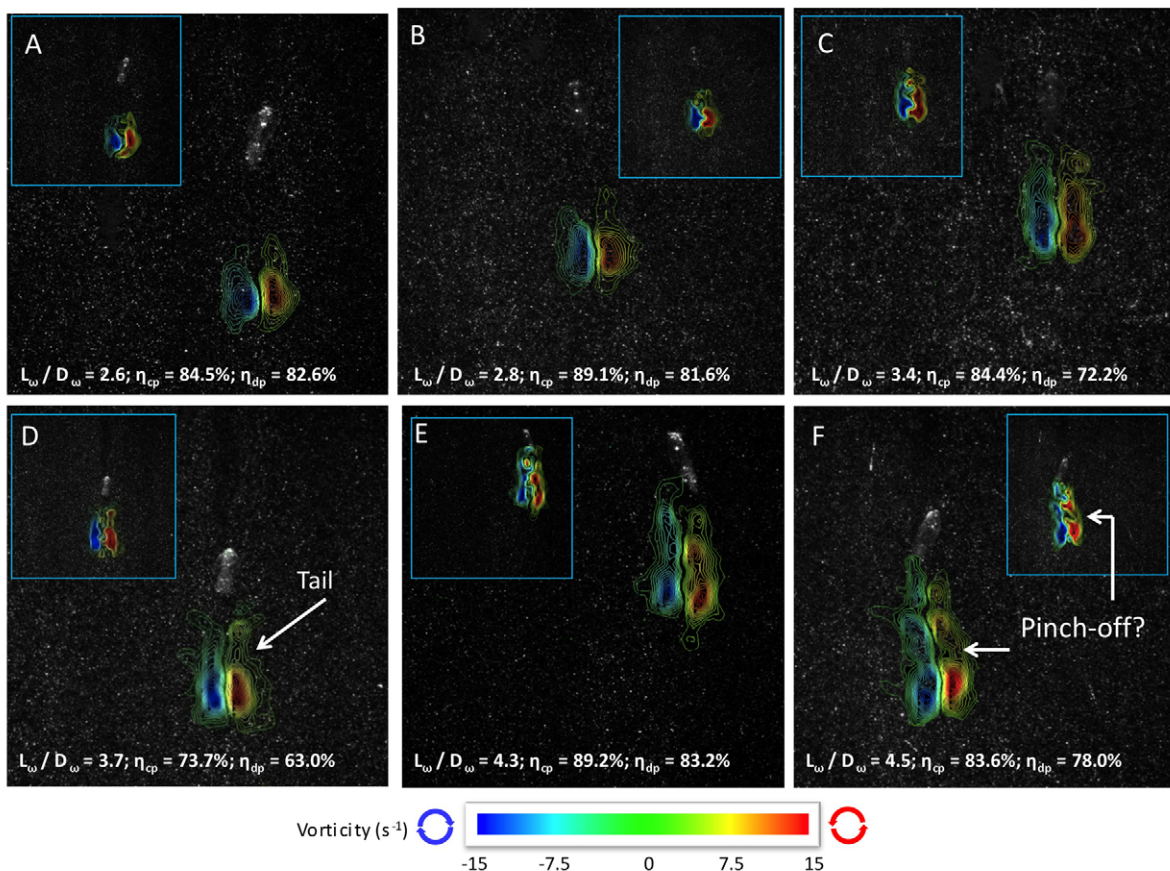
Fig. 4. Convolved vorticity fields for paralarvae *Doryteuthis pealeii* swimming at 1.4 cm s⁻¹ (7.8 *DML* s⁻¹) (A,B), 1.9 cm s⁻¹ (10.6 *DML* s⁻¹) (C), 1.2 cm s⁻¹ (6.5 *DML* s⁻¹) (D), 2.2 cm s⁻¹ (11.9 *DML* s⁻¹) (E) and 2.1 cm s⁻¹ (11.3 *DML* s⁻¹) (F). The insets represent deconvolved vorticity fields that have been adjusted for laser sheet thickness. L_ω is the length of jet based on vorticity extent, D_ω is the distance between vorticity peaks; η_{cp} is the convolved propulsive efficiency, η_{dp}=deconvolved propulsive efficiency and *DML* is the dorsal mantle length.

(Fig. 4). Spherical 'vortex rings' or 'vortex ring puffs' generally occurred at $L_\omega/D_\omega \leq 3$ [mean L_V/D_F for five jet sequences=20.7±3.2 (±s.d.), range of L_V/D_F=13.6–25.2] whereas the more elongated vortex ring structures were observed at $L_\omega/D_\omega > 3$ [mean L_V/D_F for 28 jet sequences=23.3±5.1 (±s.d.), range of L_V/D_F=17.8–36.0)], with L_ω/D_ω being a more reliable predictor of spherical vortex rings than L_V/D_F. Spherical vortex rings, i.e. $L_\omega/D_\omega \leq 3$, were less common than elongated vortex rings, i.e. $L_\omega/D_\omega > 3$ and were recorded in only 15% of the jet sequences.

L_ω/D_ω and L_V/D_F, i.e. the degree of elongation of the vortex structure, increased with mean swimming speed (U) (Table 1; Fig. 5). Mean L_ω/D_ω and L_V/D_F were 3.60±0.60 (range=2.13–4.58) and 22.7±4.81 (range=13.6–36.0), respectively. The ratio between jet velocity and swimming velocity (U_j/U and U_{jmax}/U_{max}), i.e. slip, decreased with increased swimming speed (Table 1; Fig. 5). The power law exponents (approximately –1), lack of dependence of U_j on U (Table 1; Fig. 6A) and lack of dependence of U_{jmax} on peak swimming speed (U_{max}) (Table 1; Fig. 6B) indicate that jet velocity is constant irrespective of swimming speed. Mean U_j/U was 1.61±0.73 (±s.d.) and mean U_{jmax}/U_{max} was 2.15±0.99 (±s.d.). Pulse duration increased with swimming speed (Table 1; Fig. 6C). I increased with higher L_ω/D_ω and U (Table 1; Fig. 7A,B). However, jet thrust time-averaged over the mantle contraction did not increase with L_ω/D_ω or U (Table 1; Fig. 7C,D).

Jet propulsive efficiency

Mean propulsive jet efficiency (η_p) for convolved (η_{pc}) and deconvolved (η_{pd}) data were 83.0±7.50% (range=66.0–93.6%) and 74.9±8.83% (range=56.1–87.5%), respectively. η_p increased with increased U for both convolved and deconvolved data (Table 1; Fig. 8A,B) but there was no significant dependence of η_p on L_ω/D_ω for either convolved or deconvolved data (Table 1; Fig. 8C,D).

Based on circulation of the vortex ring structures, dissipation was rapid, with complete ring dissipation occurring at ~0.5 s (Table 1; Fig. 9).

DISCUSSION
Jet structure

This study provides the first data on pulsed jet hydrodynamics of a biological organism at intermediate Re (Re_{squid}=25–90; Re_{jet}=5–25). As is the case with juvenile and adult brief squid *Lolliguncula brevis* that swim at high Re (i.e. Re>1000) (Bartol et al., 2001b; Bartol et al., 2008), vortex ring formation plays an important role in propulsion of paralarval *D. pealeii* at intermediate Re, with a continuum of vortex structures being produced from more classical spherical vortex rings to more elongated vortex rings with no clearly identifiable pinch-off. These vortex rings, which result from the separation of a boundary layer at the edge of the funnel followed by spiral roll-up of fluid, are important coherent structures because they accelerate ambient fluid downstream (either by pushing it aside or by entrainment), leading to an increased pressure at the funnel exit plane and elevated thrust per pulse (see Eqn 1) (Krueger, 2001; Krueger and Gharib, 2003). Although vortex rings have been observed and quantified around oscillatory/undulatory locomotors at intermediate Re (Müller et al., 2000; Brackenbury, 2002; van Duren and Videler, 2003), this study provides the first evidence of vortex ring structures in a jet-propelled cephalopod paralarvae. Like fish larvae, the vorticity field extent of paralarvae was large due to vorticity diffusion and vorticity dissipated quickly [within 0.5 s for paralarvae (present study), 1 s for fish larvae (Müller et al., 2000)].

Numerical and mechanically generated jet pulse studies conducted at higher Re (i.e. Re~2800–10⁴) have demonstrated the formation of vortex rings or puffs during short jets and vortex rings pinched off from the generating jet during long jets (Gharib et al., 1998;
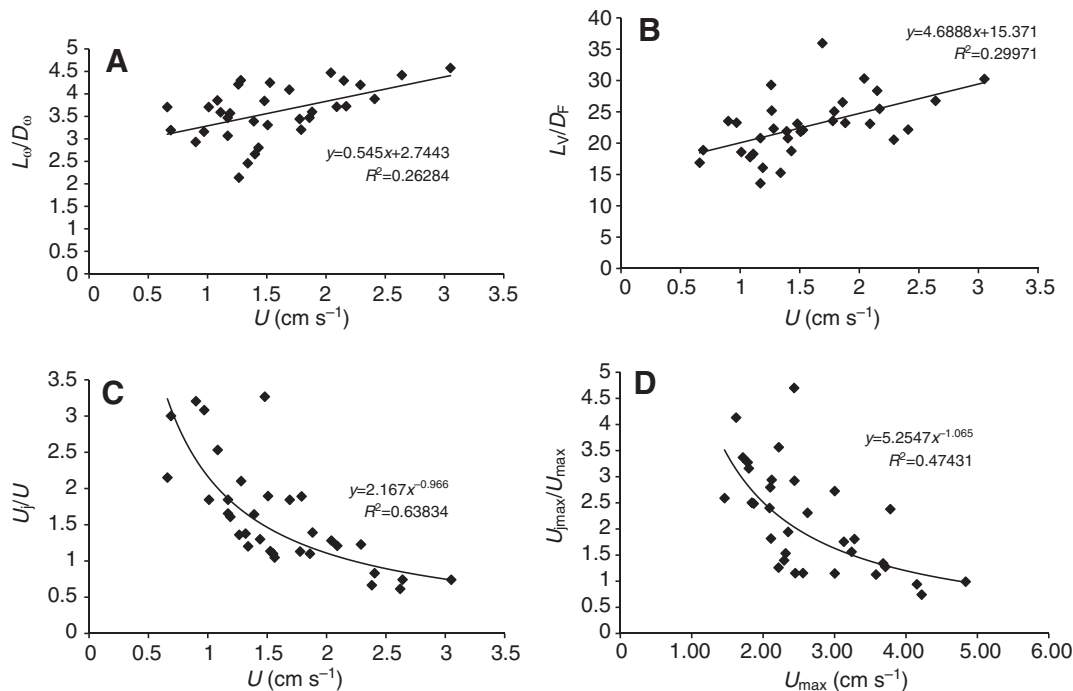
Fig. 5. Ratios of the length of jet based on the vorticity extent (L_ω) to the distance between vorticity peaks (D_ω) plotted as a function of mean swimming speed during mantle contraction (U) (A), length of the jet based on the velocity extent (L_V) to the maximum funnel diameter (D_F) plotted as a function of U (B), mean jet velocity along the jet centerline (U_j) to the mean swimming speed during mantle contraction (U) plotted as a function of U (C) and maximum jet velocity along the jet centerline (U_{jmax}) to the maximum swimming speed during mantle contraction (U_{max}) plotted as a function of U_{max} (D).

Table 1. Regression results for selected parameters

Comparison	Regression type	F	P	R^2
L_ω/D_ω on U	L	11.053	0.002*	0.262
L_v/D_F on U	L	13.268	0.001*	0.300
U_j/U on U	P	37.431	<0.0001*	0.609
U_{jmax}/U_{max} on U	P	28.836	<0.0001*	0.487
U_j on U	L	0.013	0.910	–
U_{jmax} on U_{max}	L	0.105	0.748	–
Pulse duration on U	L	18.016	<0.001*	0.368
I on L_ω/D_ω	L	11.642	0.002*	0.273
I on U	L	27.758	<0.0001*	0.472
$\tilde{F}_T$ on L_ω/D_ω	L	0.590	0.448	–
$\tilde{F}_T$ on U	L	1.632	0.211	–
η_{pc} on U	P	41.753	<0.0001*	0.574
η_{pd} on U	P	35.521	<0.0001*	0.533
η_{pc} on L_ω/D_ω	L	0.626	0.435	–
η_{pd} on L_ω/D_ω	L	0.721	0.402	–
Γ on time	L	44.799	<0.0001*	0.258

L is linear regression, P is power regression, d.f.=1, 31 for all comparisons and * denotes significance. L_ω is jet length based on the vorticity extent, D_ω is the distance between vorticity peaks, U is the mean swimming speed during mantle contraction, L_v is the jet length based on the velocity extent, D is maximum diameter of the funnel, U_j is the mean jet velocity along the jet centerline, U_{jmax} is the peak jet velocity along the jet centerline, U_{max} is the peak swimming speed, I is the jet impulse, $\tilde{F}_T$ the jet thrust time-averaged over the mantle contraction, η_{pc} is the convolved propulsive efficiency, η_{pd} is the deconvolved propulsive efficiency and Γ is jet vortex circulation.

Rosenfeld et al., 1998; Mohseni et al., 2001; Krueger and Gharib, 2005; Krueger et al., 2003; Krueger et al., 2006). These investigations revealed a limiting principle for vortex ring formation characterized in terms of F, which was introduced earlier. For

dimensionless pulse sizes beyond F, the vortex ring stops entraining circulation, impulse and energy from the generating jet and separates from the jet. F occurs when the length of the ejected fluid ($\sim L_\omega$) is about $4\times$ the diameter of the jet aperture ($\sim D_\omega$). In the present study, no clear pinch-off was observed for jets with $L_\omega/D_\omega>3$. The elongated vortex ring structures observed in the present study, however, may indeed represent a vortex ring/trailing jet complex similar to that described in Gharib et al. (Gharib et al., 1998), only that viscous diffusion has blurred the separation between the ring and jet so that 'pinch-off' is not distinguishable (see Fig. 4F). Another possibility is that the elongated vortex ring structures represent vortex rings whose formation has been pre-empted by viscous diffusion so that a vortical tail remains behind the ring (see Fig. 4D). Based on the current data set, it is not possible to make a distinction between these two possibilities but this topic certainly merits further study, involving perhaps numerical simulations or DPIV with high temporal resolution.

While the details of the evolution of the paralarval jet wake remain elusive, the observed increase in L_ω/D_ω with swimming speed indicates that longer ring structures with greater expelled water volume are integral to higher speed swimming in paralarval squid. The observed increase in L_ω/D_ω with speed is achieved by increasing pulse duration with speed, permitting a larger volume of water to be expelled and the generation of longer L_ω. Based on the results of this study, this larger volume of water is expelled at approximately the same velocity as smaller volumes of water at lower swimming speed in paralarvae, i.e. paralarvae appear to employ a relatively constant velocity jet across the speed range considered for this study. This may be related to force limitations of the mantle musculature given that specialization of sub-populations of the circular muscle fibers for high force generation in *D. pealeii* does not develop until the animals are juveniles and adults (J.T.T., P.S.K. and I.K.B., in preparation). The longer pulse durations and larger L_ω/D_ω result in
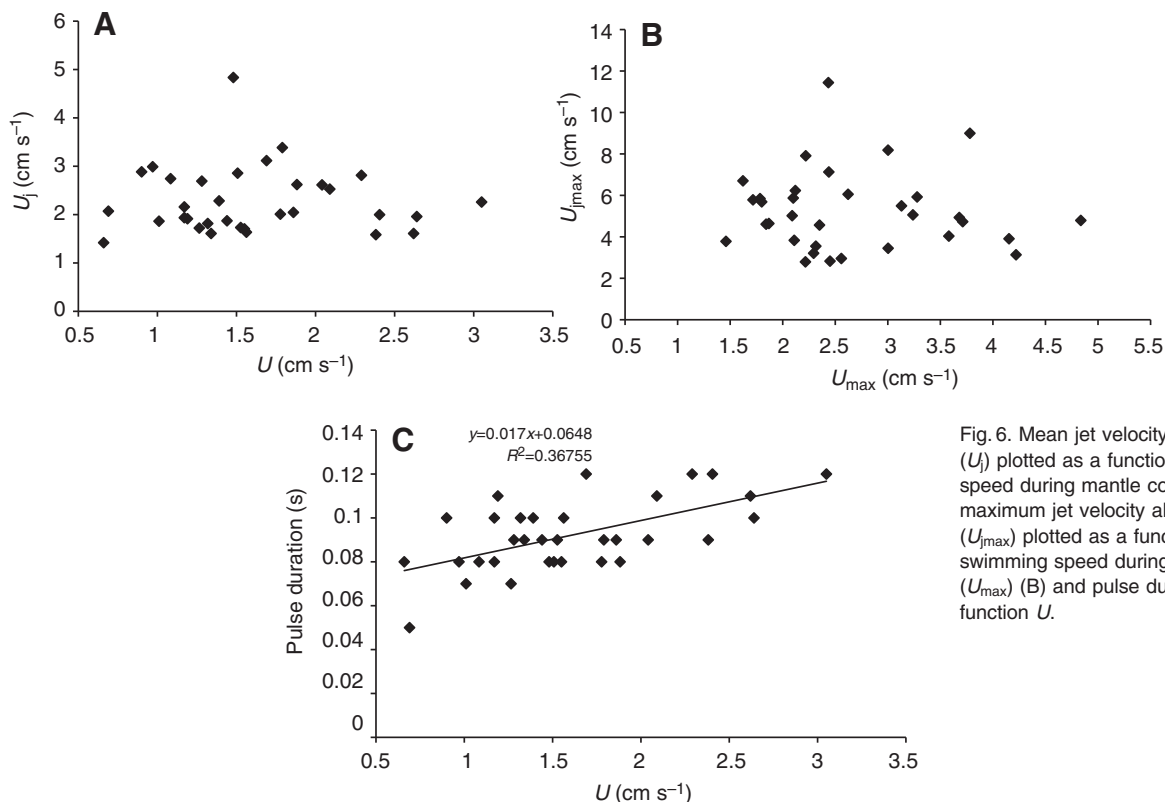
Fig. 6. Mean jet velocity along the jet centerline (U_j) plotted as a function of mean swimming speed during mantle contraction (U) (A), maximum jet velocity along the jet centerline (U_{jmax}) plotted as a function of maximum swimming speed during mantle contraction (U_{max}) (B) and pulse duration plotted as a function U.

$y=0.017x+0.0648$
$R^2=0.36755$
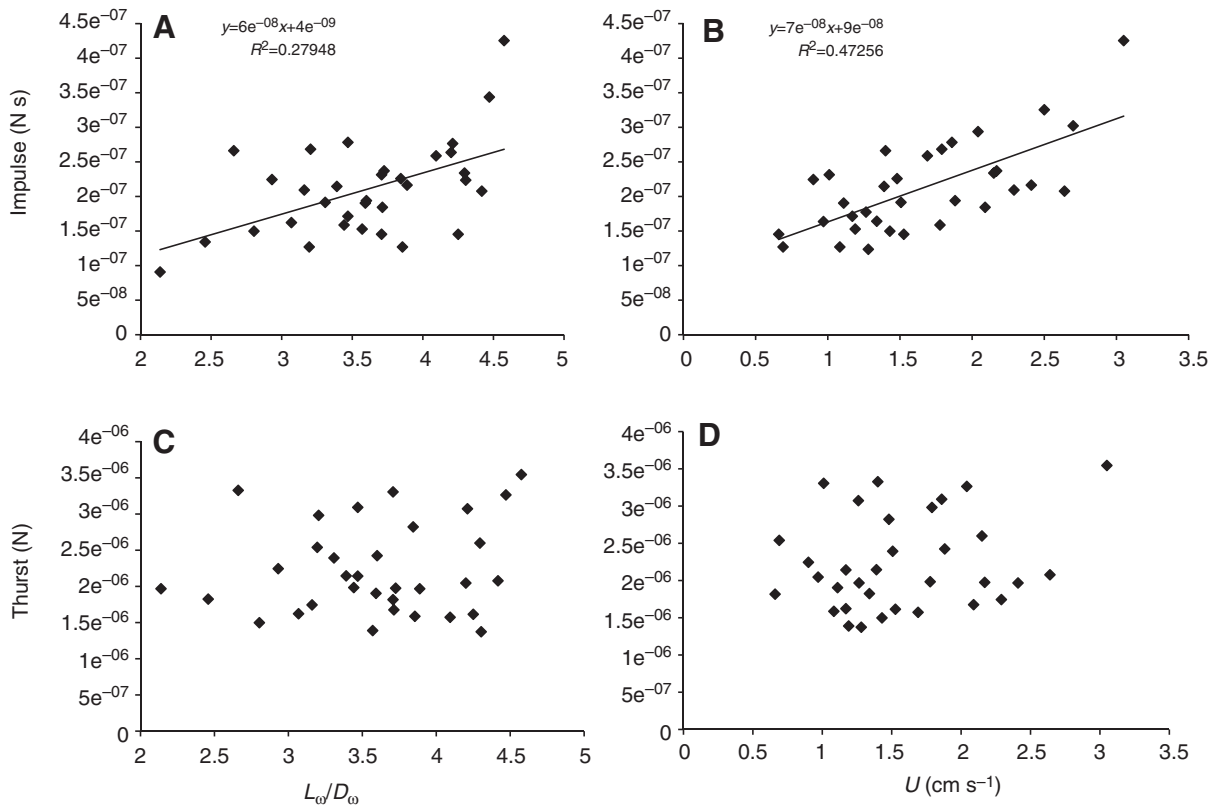
Fig. 7. Mean impulse and mean thrust plotted as a function of the ratio of jet length based on the vorticity extent to the distance between vorticity peaks (L_ω/D_ω) (A, C, respectively) and mean impulse and mean thrust plotted as a function of mean swimming speed during mantle contraction (U) (B, D, respectively).

greater impulse with speed because more jet momentum is expelled. The observed independence between thrust and speed and thrust and L_ω/D_ω can be predicted from a simple momentum analysis for a constant velocity jet. The finding that paralarvae use longer rather than faster or higher frequency jets within the speed range considered in this study is intriguing. Is this solely the product of constraints of the paralarval mantle motor system, where either the ability of the circular muscles to generate higher power or the ability of the nervous system to exert fine control over circular muscle activation is limited (see Otis and Gilly, 1990; Gilly et al., 1991)? Or, alternatively, are paralarvae employing this approach and confining their jets to a limited L_ω/D_ω to remain within a high propulsive efficiency window? Again, these questions are beyond the scope of the present study but they are interesting areas for future investigation.

One important difference between many of the mechanical jet studies described above and the present study is that squid paralarvae are self-propelled and not fixed like mechanical jet nozzles. Consequently, there is a co-flow component, i.e. external flows move over the funnel as the squid swims through the water and this will impact vortex ring formation and the resulting jet structure as discussed in other studies (see Krueger et al., 2003; Krueger et al., 2006; Anderson and Grosenbaugh, 2005). Krueger et al. (Krueger et al., 2003; Krueger et al., 2006) and Anderson and Grosenbaugh (Anderson and Grosenbaugh, 2005) both revealed that F decreases with increased uniform background co-flow at Re~1000–3000, with Krueger et al. (Krueger et al., 2003; Krueger et al., 2006) detecting a precipitous drop in F to values <1 (as opposed to values of 4) when the ratio of co-flow velocity to jet velocity (R_υ or 1/slip) is

>0.5. Krueger et al. (Krueger et al., 2006) explained the decrease in F in terms of the decreased strength of the shear layer feeding the ring and the increased rate of advection of the ring away from the nozzle as the co-flow is increased.

In the present study, well-developed spherical vortex rings were observed at L_ω/D_ω=2.1–2.9 where mean R_υ=0.76±0.26 (±s.d.) (where R_υ or 1/slip=mean swimming speed/mean jet velocity). Although these L_ω/D_ω are not exactly equivalent to the ratio of jet plug length to jet diameter (L/D) used to mechanically generate vortex rings, they are slightly higher than expected for vortex ring formation based on the findings of Krueger et al. (Krueger et al., 2003; Krueger et al., 2006). Moreover, some spherical and elongated rings formed when R_υ>1, a condition in which vortex rings should not form because the outer boundary layer presumably dominates downstream flow development. Higher L_ω/D_ω and R_υ for vortex rings reported in the present study may be a product of two important factors: (1) the present study was conducted at a lower Re realm (Re_{squid}=25–90) where viscous forces may have lowered the jet velocity somewhat from the value at the funnel aperture during jet ejection and (2) paralarvae employ muscular control of their funnel aperture during ejection, a characteristic observed in several species of squid (O'Dor, 1988; Bartol et al., 2001b; Anderson and DeMont, 2005) and other biological jetters (Dabiri et al., 2006). The investigations of co-flow components in mechanical jet studies have not incorporated temporally variable funnel apertures and, consequently, they are not fully representative of biological jetting, although they are certainly useful in providing insight into general principles related to biological propulsion. A dynamically controlled funnel probably plays a significant role in the jet structure of self-
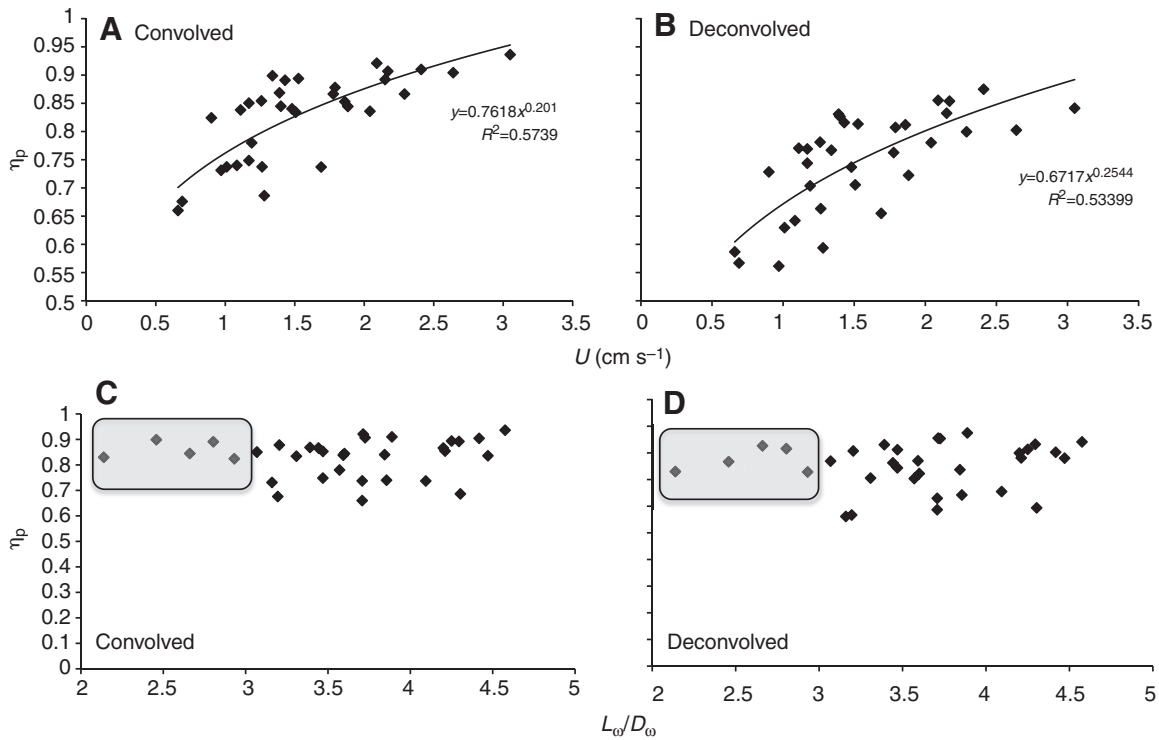
Fig. 8. Propulsive efficiency (η_p) plotted as a function of mean swimming speed during mantle contraction (U) for convolved (A) and deconvolved (B) data and propulsive efficiency (η_p) plotted as a function of the ratio of jet length based on the vorticity extent to the distance between vorticity peaks (L_ω/D_ω) for convolved (C) and deconvolved (D) data. The gray rectangles in C and D highlight values for spherical vortex rings.

propelled organisms given that Dabiri and Gharib (Dabiri and Gharib, 2005) demonstrated that funnel diameter changes in mechanical jet generators during jet ejection into stationary water contribute to higher impulse-to-energy expended ratios and higher F.

The absence of vortex ring pinch-off from a trailing jet in paralarval *D. pealeii* is intriguing when compared with the DPIV jet results of Anderson and Grosenbaugh (Anderson and Grosenbaugh, 2005) and Bartol et al. (Bartol et al., 2009). Anderson and Grosenbaugh mostly observed elongated jets [L_V/D_F=9.0–32.0 (entire jet in the field of view); L_V/D_F=5.5–61.8 (estimated jets when portions of jet were not completely visible in field of view)] with no clearly discernible leading vortex rings in adult *D. pealeii* (DML=27.1±3.0 cm) swimming over a range of speeds from 10 to 59.3 cm s^{-1} (Anderson and Grosenbaugh, 2005). Steady propulsion by individual vortex rings was not observed. In contrast to adults, *D. pealeii* paralarvae exhibited steady jetting by individual vortex rings and produced overall shorter jet pulses (L_ω/D_ω=2.1–4.8; L_V/D_F<36) that resulted in the production of spherical and elongated vortex rings with no clear pinch-off. Moreover, *Lolliguncula brevis* 3.3–9.1 cm DML in size demonstrate two distinctive jet structures or 'modes' when swimming at speeds of 2.43–22.2 cm s^{-1} (0.54 to 3.50 DML s^{-1}): (1) short jets involving isolated vortex rings (L_ω/D_ω<3, L_V/D_F=3.23–11.45) and (2) longer jets consisting of a leading vortex ring pinched off from a trailing jet (L_ω/D_ω>3, L_V/D_F=5.89–23.19) (Bartol et al., 2009). Given these findings, two important questions arise: (1) do *D. pealeii* produce fundamentally different jets than *L. brevis*, whereby leading edge vortex ring pinch-off does not occur and (2) does jet structure change significantly throughout ontogeny in squids, from paralarvae to adults? Although *D. pealeii* and *L. brevis* hatchlings are similar in morphology, they do differ significantly at older life-history stages

and thus a complete ontogenetic series of both species is required to fully address the above questions.

Propulsive efficiency

Previous studies have emphasized the importance of continuous swimming over burst-and-coast swimming at intermediate *Re*, where viscous drag lowers coasting distances significantly (Hunter, 1972; Weihs, 1974; Weihs, 1980; Batty, 1984; Webb and Weihs, 1986; Osse and Drost, 1989; Müller et al., 2000), and the importance of undulatory/oscillatory, viscous-dominated propulsion (Vlyman, 1974; Weihs, 1980; Jordan, 1992; Müller and Videler, 1996; Brackenbury, 2002; McHenry et al., 2003). Jetting in paralarvae resembles burst-and-coast swimming to some degree because there is a burst of thrust as the mantle contracts and water is expelled, followed by a coasting phase as the mantle refills. However, paralarvae are not true 'coasters' during routine station holding because they do not travel considerable distances along the direction of travel, as they fight not only viscous drag but also gravity during refilling. Paralarvae do employ a high-frequency jet, which pushes them more towards continuous swimming but they do not fall neatly into this designation either because of their mantle-refilling phase. Furthermore, paralarvae do not rely heavily on oscillatory/undulatory motions of their rudimentary fins for propulsion at early ontogenetic stages (Boletzky, 1987; Okutani, 1987; Hoar et al., 1994; Bartol et al., 2008) but rather rely almost exclusively on a pulsatile (inertial) jet.

As a result of the prominent role of viscosity at intermediate *Re* and the trend toward a relative increase in drag as *Re* decreases into the intermediate range, propulsive efficiency was expected to be low for paralarvae. However, results from the present study reveal quite the contrary. Mean η_{pc} was 83.0±7.50% (±s.d.) and mean η_{pd} was 74.9±8.83% (±s.d.). These efficiencies are not only surprisingly
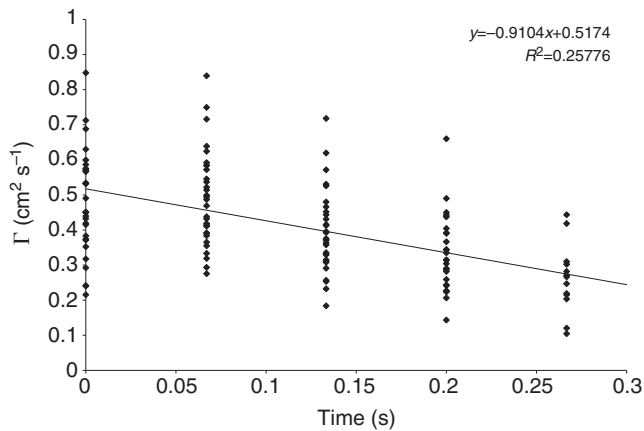
Fig. 9. Linear regression of jet vortex circulation (Γ) on time for *Doryteuthis pealeii* paralarvae.

high for a jet-propelled organism at intermediate *Re* but they are also actually higher than η_p for juvenile/adult brief squid *L. brevis* computed using Eqn 4 with impulse and kinetic energy data from other studies (see Bartol et al., 2008; Bartol et al., 2009) [mean η_p=66.5±16.3% (±s.d.); *N*=59; two-tailed *t*-test, *P*<0.01]. The efficiency advantage of paralarvae is likely to be due, in part, to their jets being more directly aligned with the direction of motion than juvenile and adult squid. Juvenile and adults squid typically have highly inclined jets especially at low swimming speed (Bartol et al., 2001b; Anderson and Grosenbaugh, 2005; Bartol et al., 2009), resulting in a lower fraction of the jet impulse doing useful work. The efficiency advantage of paralarvae is also a product of lower slip, with a mean U_j/U for paralarvae of 1.61±0.73 (±s.d.) and a mean U_j/U for juvenile/adult *L. brevis* (Bartol et al., 2009) of 2.21±1.04 (±s.d.). This lower slip may be related to two factors: morphology and over-pressure benefits. Compared with juvenile and adult squid, paralarvae have larger funnel apertures (Packard, 1969; Boletzky, 1974; Thompson and Kier, 2002) and hold proportionally greater volumes of water in their mantle cavities (Gilly et al., 1991; Preuss et al., 1997; Thompson and Kier, 2001). These characteristics allow paralarvae to expel larger volumes of water at lower speeds to produce the requisite thrust for a given normalized speed. The high pulsing rates of paralarvae relative to adult squid [mean contraction period and total jet period for paralarvae=0.092±0.016 s (±s.d.) and 0.41±0.08 s (±s.d.), respectively; mean contraction period and total jet period for juvenile and adult *L. brevis*=0.25±0.060 s (±s.d.) and 0.65±0.14 s (±s.d.), respectively (Bartol et al., 2009)], allow for the production of short jets with low L_ω/D_ω. As demonstrated by Krueger and Gharib (Krueger and Gharib, 2003), shorter jets can produce more thrust per unit of expelled fluid volume than longer duration jets because there is a higher relative contribution of over-pressure (i.e. I_P in Eqn 1) to total impulse and thrust. This thrust augmentation benefit provides the same $\overline{F}_T$ with lower I_U (see Eqn 1), allowing a lower jet velocity to be used for the same relative swimming speed.

The decrease in slip, i.e. ratio between jet velocity and swimming speed, and the accompanying increase in propulsive efficiency with increased swimming speed observed in the present study are consistent with observations of larger squids. Anderson and Grosenbaugh (Anderson and Grosenbaugh, 2005) found decreased slip and increased efficiency with speed in adult long-finned squid *D. pealeii* [mantle length (*ML*)=27.1±3.0 cm (mean±s.d.)] swimming over a range of speeds (10.1–59.3 cm s^{-1}, 0.22–2.06 *ML* s^{-1}) and

Bartol et al. (Bartol et al., 2009) observed similar trends in juvenile/adult brief squid *L. brevis* (3.3–9.1 cm *DML*) swimming at speeds of 2.43–22.2 cm s^{-1} (0.54–3.50 *DML* s^{-1}). Although not based on direct measures of the jet impulse and kinetic energy, Anderson and Grosenbaugh reported efficiencies of 86% for speeds above 0.66 *ML* s^{-1} and 93% for speeds above 1.6 *ML* s^{-1} (Anderson and Grosenbaugh, 2005). Propulsive efficiencies measured in this study for paralarval *D. pealeii* swimming at speeds above 2 cm s^{-1} (11.1 *ML* s^{-1}) were similarly high, with mean propulsive efficiencies=89.7±3.2% (±s.d.) for convolved data and 83.7±3.3% (±s.d.) for deconvolved data. The detection of such high propulsive efficiencies in both hatchling and adult *D. pealeii* is significant given the varying roles of inertia and viscosity over such a wide *Re* range (40–180,000).

The absence of a dependence of propulsive efficiency on L_ω/D_ω is not surprising considering there was no clear distinction in jet structure; a continuum of L_ω/D_ω were detected with no distinguishable pinch-off of a vortex ring from a trailing jet. The lack of dependence also may be related to the small range of observed L_ω/D_ω (2.13–4.58). The data presented in this study are for steady 'vertical bobbing' and represent the most common swimming behavior in *D. pealeii*. As the paralarvae were not forced to swim over a wide range of speeds but rather were allowed to select their own preferred speed range during vertical bobbing, the L_ω/D_ω in the present study, in all likelihood, do not represent the full range of jet structures produced by paralarvae. Escape jets, for instance, presumably involve higher L_ω/D_ω and higher Re_{jet} where pinch-off or other deviations from the observed jet structures may occur. Escape jets were not investigated in the present study because we did not have sufficient temporal resolution in our DPIV setup to reliably capture escape jets. Investigating escape jet structure is the next logical step in understanding paralarval jet structure and propulsive efficiency, however.

Jet velocity and laser sheet thickness corrections

Despite application of the deconvolution routines, mean and peak jet velocities were less than mean swimming speeds and peak swimming speeds, respectively, for the highest swimming speed sequences recorded (see Fig. 5). This may be the result of several factors. First, pulsed jet thrust is a product of both jet momentum and over-pressure (see Eqn 1). At low/intermediate *Re*, unsteady effects may be providing so much over-pressure that only low jet velocities are needed for the requisite thrust, which is certainly reasonable given greater viscous recoil resistance within the low/intermediate *Re* realm. This effect may be more pronounced at higher speed paralarval swimming. Second, viscous effects at these low/intermediate *Re* dissipate kinetic energy and lower peak jet velocities over a fairly short time scale (vortex dissipation occurred in <0.5 s in the present study). Based on the time delay between the end of jet ejection (determined from high-speed video frames of mantle and funnel diameters) and the first measurement of kinetic energy (~0.02 s), mean dissipation for kinetic energy was 7.8±4.3% (±s.d.). Although it is not possible to calculate the associated velocity reduction, the jet velocity decrease could lead to slip values below 1. Third, application of the deconvolution may have imperfectly corrected the centerline velocity due to non-axisymmetric features near the centerline.

Morphology, muscle mechanics and ecology

Squid paralarvae have several morphological characteristics that aid them in their vertical station holding lifestyle. Compared with juvenile and adult squid, paralarvae have relatively larger funnel apertures (Packard, 1969; Boletzky, 1974; Thompson and Kier,

2002) and hold proportionally greater volumes of water in their mantle cavities (Gilly et al., 1991; Preuss et al., 1997; Thompson and Kier, 2001): features that permit the ejection of high-volume, low-velocity flow for a given swimming speed. *Sepioteuthis lessoniana* paralarvae do, in fact, expel relatively larger volumes of water through their large apertures at low velocities, produce lower peak mass-specific thrust and generate higher relative mass flux than do adults during escape jetting (Thompson and Kier, 2001; Thompson and Kier, 2002). The low slip values detected in the present study are consistent with these findings.

In both *S. lessoniana* and *D. pealeii*, the thick filaments of the mantle muscles that provide power for jetting (i.e. the circular muscles) are 1.5–2.5-fold longer in juveniles and adults than in paralarvae (Thompson and Kier, 2006; J.T.T., P.S.K. and I.K.B., in preparation). Because shortening velocity is proportional to the number of sarcomeres in series (e.g. Josephson, 1975) and shorter thick filaments potentially allow more sarcomeres per unit length of muscle fiber, the shorter thick filaments of paralarval circular muscle fibers may permit more rapid mantle contractions, assuming that other aspects of the muscles are the same. These rapid mantle contractions allow for more continuous swimming and less coasting, which is beneficial at intermediate *Re* where viscosity is prominent and coasting is inhibited. This prediction is consistent with the mantle contraction times described in the Results above and the observation of significantly higher maximum unloaded shortening velocities in the central mitochondria poor and superficial mitochondria rich circular muscle fibers of paralarval *D. pealeii* relative to adults (J.T.T., P.S.K. and I.K.B., in preparation). The ontogenetic change in the thick filament lengths of the circular fibers is not accompanied by a change in the expression of isoforms of myosin heavy chain (J.T.T., P.S.K. and I.K.B., in preparation). Thus, the rapid mantle contractions and short jet periods that are important for generating high propulsive efficiency in paralarvae appear to result from an ultrastructural specialization of the circular muscle fibers.

Within a day or two of hatching, squid paralarvae are competent predators, having the ability to attack and consume live prey of appropriate sizes (Mangold and Boletzky, 1985; Nabhitabhata et al., 2001; Hanlon, 1990). Paralarvae are predominantly vertical migrators, depending heavily on currents for horizontal displacement (Fields, 1965; Sidie and Halloway, 1999; Zeidberg and Hamner, 2002; Boyle and Rodhouse, 2005), with some paralarvae undergoing daily vertical migrations of 15 m while being entrained within cyclonic gyres near shore waters (Zeidberg and Hamner, 2002). Therefore, it is not surprising that the paralarvae in the present study employed a largely vertical jet while station holding in the holding chamber. Even while holding position in the water column, paralarvae were capable of impressive speeds during mantle contraction; average swimming speed was $2.68 \pm 0.85\,\mathrm{cm\,s^{-1}}$ ($\pm$s.d.) [$14.74 \pm 4.56\,DML\,\mathrm{s^{-1}}$ ($\pm$s.d.)] during mantle contraction with a range of 1.46–$4.84\,\mathrm{cm\,s^{-1}}$ (4.98–$26.87\,DML\,\mathrm{s^{-1}}$). Although holding position and vertically migrating are preferred behaviors, paralarvae are also capable of escape jetting and can achieve high speeds. *Loligo vulgaris, Doryteuthis opalescens* and *D. pealeii* paralarvae can reach speeds of 12–$16\,\mathrm{cm\,s^{-1}}$ (26.7–$83.3\,DML\,\mathrm{s^{-1}}$) during escape jetting (Packard, 1969; Preuss et al., 1997; J.T.T., P.S.K. and I.K.B., in preparation) whereas *Illex illecebrosus* paralarvae can reach speeds of $5.0\,\mathrm{cm\,s^{-1}}$ ($27.8\,DML\,\mathrm{s^{-1}}$) (O'Dor et al., 1986). These escape jets are important for paralarvae for evading predators and attacking prey. As indicated earlier, DPIV analyses of escape jets were not performed because of temporal limitations but such studies would provide valuable data at the upper limit of paralarval jetting.

Concluding remarks

Vortex ring structures clearly play a prominent role in locomotion of paralarval *D. pealeii*, with a continuum of such structures being produced during jetting from spherical (classic) vortex rings to more elongated rings. At the intermediate *Re* range of swimming paralarvae, no clear pinch-off of a leading vortex ring from a longer trailing jet was present even at the largest L_ω / D_ω observed, which differs from results from mechanical jet studies and some live-animal adult squid studies at higher *Re*. Interestingly, paralarvae swim faster by producing longer rather than faster jets; this may result from mantle motor system constraints or selection for high propulsive efficiency at a variety of swimming speeds. Despite previous expectations of low propulsive efficiency at intermediate *Re*, our results revealed that paralarvae actually have high propulsive efficiency and low slip during their vertical bobbing behaviors, especially at high speeds. High jet propulsive efficiency may be more important for paralarvae than older life-history stages because their fins play such a minor role in propulsion relative to the contributions of the highly efficient fins of juveniles and adults (Bartol et al., 2008), requiring paralarvae to rely more heavily on their jet for propulsion. Therefore, although paralarvae may represent the lower size limit of biological jet propulsion, they do not denote the lower propulsive efficiency limit to biological jet propulsion. Paralarvae achieve unexpectedly high levels of propulsive efficiency through the production of high-frequency, high-volume, low-velocity jets that reduce excess kinetic energy and presumably provide considerable over-pressure benefits.

LIST OF ABBREVIATIONS

C_D	drag coefficient
D	diameter of mechanical jet aperture
D_F	maximum diameter of funnel
DML	dorsal mantle length
DPIV	digital particle image velocimetry
D_ω	distance between vorticity peaks
E	excess kinetic energy of the jet
f	actual data field being averaged
F	formation number
$\bar{F}_T$	time-averaged thrust
$\tilde{F}_T$	jet thrust time-averaged over the mantle contraction
I	jet impulse
I_P	impulse per pulse supplied by nozzle exit over-pressure
I_U	impulse per pulse supplied by jet momentum flux
k	convolution kernel
L	length of ejected plug of fluid
L_b	body length
L_V	jet length based on the velocity extent
L_ω	jet length based on the vorticity extent
ML	mantle length
$\hat{\mathbf{n}}_r$	unit vector in the radial direction relative to the jet centerline
$\hat{\mathbf{n}}_z$	unit vector in the longitudinal direction along the jet centerline
r	radial coordinate
Re	Reynolds number
Re_{jet}	Reynolds number of jet
Re_{squid}	Reynolds number of squid
R_υ	ratio of co-flow velocity to jet velocity
t	laser sheet thickness
T	period between successive jets
$\langle u_r \rangle$	convolved (i.e. measured) radial velocity
u_r	actual radial velocity

$\langle u_z \rangle$	convolved (i.e. measured) axial velocity
u_z	actual axial velocity
U	mean swimming speed
$\hat{U}$	swimming speed normalized in body lengths s^{-1}
U_j	mean jet velocity along the jet centerline
U_{jmax}	peak jet velocity along the jet centerline
U_{max}	peak swimming speed
x	displacement during mantle contraction
z	longitudinal coordinate along the jet centerline
Γ	jet vortex circulation
η_p	propulsive jet efficiency
η_{pc}	convolved propulsive efficiency
η_{pd}	deconvolved propulsive efficiency
$\theta_r(\tau)$	angle between the 3-D radial direction relative to the jet axis and the vertical plane of the center of the laser sheet at location τ within the laser sheet
ρ	fluid density
ψ	Stokes stream function
ω_θ	azimuthal component of vorticity

REFERENCES

Anderson, E. J. and DeMont, M. E. (2005). The locomotory function of the fins in the squid *Loligo pealei*. *Mar. Freshw. Behav. Phys.* **38**, 169-189.

Anderson, E. J. and Grosenbaugh, M. A. (2005). Jet flow in steadily swimming adult squid. *J. Exp. Biol.* **208**, 1125-1146.

Bartol, I. K., Mann, R. and Patterson, M. R. (2001a). Aerobic respiratory costs of swimming in the negatively buoyant brief squid *Lolliguncula brevis*. *J. Exp. Biol.* **204**, 3639-3653.

Bartol, I. K., Patterson, M. R. and Mann, R. (2001b). Swimming mechanics and behavior of the negatively buoyant shallow-water brief squid *Lolliguncula brevis*. *J. Exp. Biol.* **204**, 3655-3682.

Bartol, I. K., Krueger, P. S., Thompson, J. T. and Stewart, W. J. (2008). Swimming dynamics and propulsive efficiency of squids throughout ontogeny. *Integr. Comp. Biol.*, **48**, 720-733.

Bartol, I. K., Krueger, P. S., Stewart, W. J. and Thompson, J. T. (2009). Hydrodynamics of pulsed jetting in juvenile and adult brief squid *Lolliguncula brevis*: evidence of multiple jet 'modes' and their implications for propulsive efficiency. *J. Exp. Biol.* (in press).

Batty, R. S. (1984). Development of swimming movements and musculature of larval herring (*Clupea harengus*). *J. Exp. Biol.* **110**, 217-229.

Boletzky, S. V. (1974). The "larvae" of cephalopoda: a review. *Thalassia Jugosl.* **10**, 45-76.

Boletzky, S. V. (1987). Embryonic phase. In *Cephalopod Life Cycles,* vol. 2 (ed. P. R. Boyle), pp. 5-31. London: Academic Press.

Borrell, B. J., Goldbogen, J. A. and Dudley, R. (2005). Aquatic wing flapping at low Reynolds numbers: swimming kinematics of the Antarctic pteropod, *Clione Antarctica*. *J. Exp. Biol.* **208**, 2939-2949.

Boyle, P. and Rodhouse, P. (2005). *Cephalopods: Ecology and Fisheries*. Oxford: Blackwell Science.

Brackenbury, J. (2002). Kinematics and hydrodynamics of an invertebrate undulatory swimmer: the damsel-fly larva. *J. Exp. Biol.* **205**, 627-639.

Catton, K. B., Webster, D. R., Brown, J. and Yen, J. (2007). Quantitative analysis of tethered and free-swimming copepodid flow fields. *J. Exp. Biol.* **210**, 299-310.

Dabiri, J. O. and Gharib, M. (2005). Starting flow through nozzles with temporally variable exit diameter. *J. Fluid. Mech.* **538**, 111-136.

Dabiri, J. O., Colin, S. P. and Costello, J. H. (2006). Fast-swimming hydromedusae exploit velar kinematics to form an optimal vortex wake. *J. Exp. Biol.* **209**, 2025-2033.

Fields, W. G. (1965). The structure, development, food relations, reproduction, and life history of the squid *Loligo opalescens* Berry. *Fish. Bull. Calif. Fish. Game.* **131**, 1-108.

Fuiman, L. A. and Batty, R. S. (1997). What a drag it is getting cold: partitioning the physical and physiological effects of temperature on fish swimming. *J. Exp. Biol.* **200**, 1745-1755.

Gharib, M., Rambod, E. and Shariff, K. (1998). A universal time scale for vortex ring formation. *J. Fluid. Mech.* **360**, 121-140.

Gilly, W. F., Hopkins, B. and Mackie, G. O. (1991). Development of giant motor axons and neural control of escape responses in squid embryos and hatchlings. *Biol. Bull.* **180**, 209-220.

Hanlon, R. T. (1990). Maintenance, rearing and culture of teuthoid and sepiod squids. In *Squid as Experimental Animals* (ed. D. L. Gilbert, W. J. Adelman and J. M. Arnold), pp. 35-62. New York: Plenum Press.

Hoar, J. A., Sim, E., Webber, D. M. and O'Dor, R. K. (1994). The role of fins in the competition between squid and fish. In *Mechanics and Physiology of Animal Swimming* (ed. L. Maddock, Q. Bone and J. M. C Rayner), pp. 27-33. Cambridge: Cambridge University Press.

Hunter, J. R. (1972). Swimming and feeding behaviour of larval anchovy *Engraulis mordax*. *Fish. Bull.* **70**, 821-838.

Jordan, C. (1992). A model of rapid-start swimming at intermediate Reynolds number: undulatory locomotion in the chaetognath *Sagitta elegans*. *J. Exp. Biol.* **163**, 119-137.

Josephson, R. K. (1975). Extensive and intensive factors determining the performance of striated muscle. *J. Exp. Zool.* **194**, 135-154.

Krueger, P. S. (2001). The significance of vortex ring formation and nozzle exit over-pressure to pulsatile jet propulsion. PhD thesis, California Institute of Technology, Pasadena, CA, USA.

Krueger, P. S. and Gharib, M. (2003). The significance of vortex ring formation to the impulse and thrust of a starting jet. *Phys. Fluids* **15**, 1271-1281.

Krueger, P. S. and Gharib, M. (2005). Thrust augmentation and vortex ring evolution in a fully-pulsed jet. *AIAA J.* **43**, 792-801.

Krueger, P. S., Dabiri, J. O. and Gharib, M. (2003). Vortex ring pinchoff in the presence of simultaneously initiated uniform background co-flow. *Phys. Fluids* **15**, L49-L52.

Krueger, P. S., Dabiri, J. O. and Gharib, M. (2006). The formation number of vortex rings formed in uniform background co-flow. *J. Fluid Mech.* **556**, 147-166.

Malkiel, E., Sheng, J., Katz, J. and Strickler, J. R. (2003). The three-dimensional flow field generated by a feeding calanoid copepod measured using digital holography. *J. Exp. Biol.* **206**, 3657-3666.

Mangold, K. and Boletzky, S. V. (1985). Biology and distribution of early juvenile cephalopods. *Vie Milieu* **35**, 304.

McHenry, M. J., Azizi, E. and Strother, J. A. (2003). The hydrodynamics of locomotion at intermediate Reynolds numbers: undulatory swimming in ascidian larvae (*Botrylloides* sp.). *J. Exp. Biol.* **206**, 327-343.

Mohseni, K., Ran, H. and Colonius, T. (2001). Numerical experiments on vortex ring formation. *J. Fluid Mech.* **430**, 267-282.

Müller, U. K. and Videler, J. J. (1996). Inertia as a 'safe harbour': do fish larvae increase length growth to escape viscous drag? *Rev. Fish Biol. Fish.* **6**, 353-360.

Müller, U. K., Stamhuis, E. J. and Videler, J. J. (2000). Hydrodynamics of unsteady fish swimming and the effects of body size: comparing the flow field of fish larvae and adults. *J. Exp. Biol.* **203**, 193-206.

Nabhitabhata, J., Asawangkune, P., Amornjaruchit, S. and Promboon, P. (2001). Tolerance of eggs and hatchlings of neritic cephalopods to salinity changes. *Phuket Mar. Biol. Cent. Spec. Publ.* **25**, 91-99.

O'Dor, R. K. (1988). Forces acting on swimming squid. *J. Exp. Biol.* **137**, 421-442.

O'Dor, R. K., Balch, N., Foy, E. A. and Helm, P. L. (1986). The locomotion and energetics of hatchling squid, *Illex illecebrosus*. *Am. Malacol. Bull.* **4**, 55-60.

Okutani, T. (1987). Juvenile morphology. In *Cephalopod Life Cycle*s, vol. 2 (ed. P. R. Boyle). Miami, FL: Associated Press.

Osse, J. W. M. and Drost, M. R. (1989). Hydrodynamics and mechanics of fish larvae. *Pol. Arch. Hydrobioil.* **36**, 455-465.

Otis, T. S. and Gilly, W. F. (1990). Jet-propelled escape in the squid *Loligo opalescens*: concerted control by giant and non-giant motor axon pathways. *Proc. Natl. Acad. Sci. USA* **87**, 2911-2915.

Packard, A. (1969). Jet propulsion and the giant fibre response of *Loligo*. *Nature* **221**, 875-877.

Preuss, T., Lebaric, Z. N. and Gilly, W. F. (1997). Post-hatching development of circular mantle muscles in the squid *Loligo opalescens*. *Biol. Bull.* **192**, 375-387.

Rosenfeld, M., Rambod, E. and Gharib, M. (1998). Circulation and formation number of laminar vortex rings. *J. Fluid Mech.* **376**, 297-318.

Sidie, J. and Holloway, B. (1999). Geotaxis in the squid hatchling *Loligo pealei*. *Am. Zool.* **39**, 74A.

Thompson, J. T. and Kier, W. M. (2001). Ontogenetic changes in mantle kinematics during escape-jet locomotion in the oval squid, *Sepioteuthis lessoniana* Lesson, 1830. *Biol. Bull.* **201**, 154-166.

Thompson, J. T. and Kier, W. M. (2002). Ontogeny of squid mantle function: changes in the mechanics of escape-jet locomotion in the oval squid, *Sepioteuthis lessoniana* Lesson, 1830. *Biol. Bull.* **203**, 14-26.

Thompson, J. T. and Kier, W. M. (2006). Ontogeny of mantle musculature and implications for jet locomotion in oval squid *Sepioteuthis lessoniana*. *J. Exp. Biol.* **209**, 433-443.

Van Duren, L. A. and Videler, J. J. (2003). Escape from viscosity: the kinematics and hydrodynamics of copepod foraging and escape swimming. *J. Exp. Biol.* **206**, 269-279.

Vecchione, M., Shea, E., Bussarawit, S., Anderson, F., Alexeyev, D., Lu, C. C., Okutani, T., Roeleveld, M., Chotiyaputta, C., Roper, C. et al. (2005). Systematic of Indo-West Pacific loliginids. Phuket. *Mar. Biol. Cent. Res. Bull.* **66**, 23-26.

Vlyman, W. J. (1974). Swimming energetics of the larval anchovy, *Engraulis mordax*. *Fish. Bull.* **72**, 885-899.

Webb, P. W. and Weihs, D. (1986). Functional locomotor morphology of early life history stages of fishes. *Trans. Am. Fish. Soc.* **115**, 115-127.

Weihs, D. (1974). Energetic advantages of burst swimming of fish. *J. Theor. Biol.* **48**, 215-229.

Weihs, D. (1980). Energetic significance of changes in swimming modes during growth of larval anchovy, *Engraulis mordax*. *Fish. Bull.* **77**, 597-604.

Westerweel, J., Dabiri, D. and Gharib, M. (1997). The effect of a discrete window offset on the accuracy of cross-correlation analysis of digital PIV recordings. *Exp. Fluids* **23**, 20-28.

White, F. M. (2006). *Viscous Fluid Flow*, 3rd edn. New York: McGraw-Hill.

Willert, C. E. and Gharib, M. (1991). Digital particle image velocimetry. *Exp. Fluids* **10**, 181-193.

Williams, T. A. (1994). A model of rowing propulsion and the ontogeny of locomotion in *Artemia* larvae. *Biol. Bull.* **187**, 156-163.

Yen, J. and Fields, D. M. (1992). Escape responses of *Acartia hudsonica* (copepoda) nauplii from the flow field of *Temora longicornis* (copepoda). *Arch. Hydrobiol. Beih. Ergebn. Limnol.* **36**, 123-134.

Young, R. E. and Harman, R. F. (1988). 'Larva', 'paralarva', and 'sub-adult' in cephalopod terminology. *Malacologia* **29**, 201-207.

Zeidberg, L. D. and Hamner, W. M. (2002). Distribution of squid paralarvae, *Loligo opalescens* (Cephalopoda: Myopsida), in the southern California Bight in the three years following the 1997-1998 El Nino. *Mar. Biol.* **141**, 111-122.